Accepted Manuscript

Probing the effects of thermal treatment on the electronic structure and mechanical properties of Ti-doped ITO thin films

Hatem Taha, David J. Henry, Chun Yang Yin, Amun Amri, Xiaoli Zhao, Syaiful Bahri, Cam Le Minh, Nguyen Ngoc Ha, M. Mahbubur Rahman, Zhong-Tao Jiang

PII: S0925-8388(17)31981-3

DOI: 10.1016/j.jallcom.2017.06.007

Reference: JALCOM 42075

To appear in: *Journal of Alloys and Compounds*

Received Date: 15 February 2017

Revised Date: 15 May 2017

Accepted Date: 1 June 2017

Please cite this article as: H. Taha, D.J. Henry, C.Y. Yin, A. Amri, X. Zhao, S. Bahri, C. Le Minh, N.N. Ha, M.M. Rahman, Z.-T. Jiang, Probing the effects of thermal treatment on the electronic structure and mechanical properties of Ti-doped ITO thin films, *Journal of Alloys and Compounds* (2017), doi: 10.1016/j.jallcom.2017.06.007.

Probing the effects of thermal treatment on the electronic structure and mechanical properties of Ti-doped ITO thin films

Hatem Taha[a,b], David J. Henry[c], Chun Yang Yin[d], Amun Amri[e], Xiaoli Zhao[f], Syaiful Bahri[e], Le Minh Cam[g], Nguyen Ngoc Ha[g], M. Mahbubur Rahman[h], Zhong-Tao Jiang[a*]

[a] Surface Analysis and Materials Engineering Research Group, School of Engineering and Information Technology, Murdoch University, Perth, WA 6150, Australia
[b]College of Ibn-Alhaitham for pure science, University of Baghdad, Baghdad, Iraq
[c]Chemical and Metallurgical Engineering and Chemistry, School of Engineering and Information Technology, Murdoch University, Perth, WA 6150
[d]Newcastle University Singapore, SIT Building @Ngee Ann Polytechnic, 537 Clementi Road #06-01, Singapore 599493
[e]Department of Chemical Engineering, University of Riau, Pekanbaru, Indonesia
[f]School of Engineering, Edith Cowan University, Joondalup, WA 6027, Australia
[g]Faculty of Chemistry, Hanoi National University of Education, Building A4, 136 Xuan Thuy Road, Cau Giay Dist. Hanoi, Vietnam
[h]Department of Physics, Jahangirnagar University, Savar, Dhaka 1342, Bangladesh

*Corresponding Author: Corresponding author. Tel.: +61 8 9360 2867.
Email address: Z.Jiang@murdoch.edu.au (Z-T Jiang)

Keywords: Transparent conductive oxide, ITO, titanium doped indium tin oxide, sol-gel, thermal treatment, X-ray photoelectron spectroscopy

Abstract

Titanium-doped indium tin oxide thin films were synthesized *via* a sol-gel spin coating process. Surface chemical bonding states and mechanical properties have been investigated as a function of titanium content (2 and 4 at%) and annealing temperature ranging from 400 to 600°C with increments of 100°C. Raman analysis was performed to study the phonon vibrations for the prepared samples and the results revealed the existence of ITO vibrational modes. The elemental compositions, bonding states and binding energies of the film materials were investigated using X-ray photoelectron spectroscopy (XPS) technique. The XPS results indicated that the ratio of the metallic elements (In, Sn, Ti) to the oxygen on the surface of the thin film coatings decreased due to the increase of the oxide layer on the surface of the thin films. Also, by increasing the annealing temperature up to 600°C, the Ti 2p and Cl 2p signals were no longer detected for both 2 and 4 at% Ti contents, due to the thicker surface oxidation layer. Mechanical properties of the synthesized films were also evaluated using a nanoindentation process. Variations in the hardness (*H*) and the elastic modulus (*E*) were observed with different Ti at% and annealing temperatures. The hardness is within the range of 6.3-6.6 GPa and 6.7-6.8 GPa for 2 and 4 at% Ti content samples, respectively, while the elastic modulus is within the ranges of 137-143 and 139-143 GPa for 2 at% and 4 at% Ti contents samples, respectively. A combination of the highest *H* and *E* were achieved in the sample of 4% Ti content annealed at 600 °C. Furthermore, the *H/E* ratio ranges from 4.5×10^{-2} to 5.0×10^{-2} which reflects a reasonable level of wear resistance.

1. Introduction

Transparent conductive oxides (TCOs) receive widespread attention from researchers due to their unique combination of very low electrical resistivity and high optical transparency over the visible spectral region [1-4]. They exhibit favorable properties which include high infrared reflection, good chemical stability and good mechanical properties along with low electrical contact resistance and high optical transparency in the visible light region. Indium oxide (In_2O_3) and/or indium tin oxide (ITO) based TCOs are the most commonly used transparent conductive oxides compared with zinc oxide (ZnO), aluminium doped zinc oxide (AZO), tin oxide (SnO_2), and cadmium oxide (CdO) [5, 6]. ITO-based TCO films can exhibit different electro-optical, mechanical, electronic structure and composition properties depending on manufacturing technique. Many deposition techniques are used to prepare TCO coatings such as Dc and/or RF sputtering, chemical vapour deposition, reactive evaporation, molecular beam epitaxy, sol-gel method, electron beam evaporation and pulsed laser deposition [7-14]. However, the sol-gel technique has many advantages including cost effectiveness, short processing time, simplicity and the opportunity to fabricate coatings with high scalability along with the flexibility of fine-tuning coatings to have preferred shapes and surface areas [15-18].

Novel ITO composites doped with 3-d and/or 4-d transition metals, such as (Ti, Ag, Cr, Mo, W, Ta and Cu), are being considered as potential candidates in a wide range of optoelectronic applications such as organic and inorganic solar cells, touch screens, organic light-emitting diodes, sensors and electro-chromic devices [19-24]. In order to satisfy the demands for some of these applications, TCO composites with improved durability are required. The durability of ITO based coatings depends on their physical, mechanical and structural properties. Therefore, it is expected that the mechanical properties of ITO based films play a significant role in the performance of optoelectronic devices. It has been reported that the bare ITO films have a brittle surface and seem to be susceptible to cracking and delamination. So far, there has been scarce information on the mechanical properties of ITO thin films, particularly,

their micro or nanostructure. The elastic modulus and the hardness of 240 nm thick sputtered ITO thin film coatings were reported by Chen *et.al* [20] to be 140 GPa and 12 GPa respectively. The hardness and elastic modulus were enhanced by introducing hydrogen into the gas mixture during the deposition process [25]. We propose that incorporating a transition metal such as titanium into the ITO nanostructure may enhance the mechanical properties of this material. Therefore, the main objective of the present study is to evaluate the influence of variations in the Ti concentration and annealing temperature on the chemical bonding states and the mechanical properties, including Young's modulus (*E*) and Hardness (*H*) of spin coated Ti-doped ITO thin films, technical aspects which have not been reported thus far, to the best of the authors' knowledge.

2. Experimental details

2.1. Thin films deposition

Hydrated indium nitrate ($In(NO_3)_3 \cdot 5H_2O$, purity 99.9%, Alfa Aesar) titanium(IV) isopropoxide ($Ti[OCH(CH_3)_2]_4$, purity 99.9%, Sigma Aldrich), and tin chloride dihydrate ($SnCl_2 \cdot 2H_2O$, purity 98%, Chem-supply) were used as received as precursors to produce Ti-doped ITO films *via* a sol-gel spin coating process. Absolute ethanol was used as a solvent and the ITO films were deposited onto soda-lime glass slides.

ITO solutions (0.1 M) were prepared by dissolving appropriate amounts of $In(NO_3)_3 \cdot 5H_2O$ and $SnCl_2 \cdot 2H_2O$ separately in absolute ethanol. The solutions were combined and stirred vigorously for 1 hour. Required amounts of ($Ti[OCH(CH_3)_2]_4$) were then dissolved in ethanol and added to ITO solutions in order to obtain solutions of Ti doped ITO with 2 and 4 at% Ti contents, respectively. The resultant solutions were then refluxed at 85°C for 1 hour and aged for 24 hours at room temperature. Since uniformity and homogeneity of the thin films mainly depends on the cleanness of the substrates, the glass substrates with (25×25 mm dimensions) were first washed with soap and rinsed repeatedly in deionized water. Then, the substrates were sonicated at 60 °C for 10 min in ethanol and DI water, respectively and dried in a vacuum drying oven at 100 °C, prior to the coating process. A Polos spin coater was used to fabricate Ti-doped

ITO films based on three main spin steps. Firstly, the solution was dispensed on to the substrate at 300 rpm for 15 seconds followed by spreading at 2500 rpm for 20 seconds and finally dried at 4000 rpm for 20 seconds. The sample was calcined on a conventional hot plate at 150 °C for 10 minutes. These steps were repeated until the desired coating thickness (300 – 400 nm) was achieved. Thermal annealing in air atmosphere was performed upon the fabricated samples at (400, 500 and 600) °C for 2h. Figure 1 is the flow chart for Ti doped ITO thin films preparation via sol-gel spin coating technique.

2.2. Characterization techniques

Raman analysis was performed on a Nicolet 6700 Fourier transform infrared (FT-IR) spectrophotometer attached with an NXR FT-Raman module. Raman spectra were obtained by using the following settings: Helium-Neon (He-Ne) laser beam with excitation wavelength and operation power of 1064 nm and 0.204 W, respectively, InGaAs detector with 90° detection angle, optical velocity of 0.3165, CaF_2 beam splitter, gain of 1, aperture of 150, maximum peak to peak signal along with optimum focusing and side-to-side values, and 32 scans with resolution of 8 cm^{-1} in the range of 0-4000 cm^{-1}. Information of elemental compositions, chemical structures and bonding states of the thin film coating surfaces were probed using a Kratos Axis Ultra-X-ray Photoelectron Spectrometer. The X-ray source was Al-Kα monochromatic radiation ($h\nu$ = 1486.6 eV) with a power of 15 kV and 10 mA. The base pressure of the analysis chamber maintained at 2.9×10^{-9} Torr. The XPS survey and high resolution scans were collected before etching. Typical high resolution XPS core level spectra were focused on the regions of In3d, Sn3d, Ti2p, O1s and C1s. The deconvolution of high resolution spectra was carried by employing the CASA XPS software (version 2.3.1.5) which provides information for the analyses of chemical bonding states.

The elastic modulus (E) and the hardness (H) of the coatings were measured using a nanoindentation workstation (Ultra-Micro Indentation System 2000, CSIRO, Sydney, Australia), equipped with a diamond Berkovich indenter [26]. The area function of the indenter tip was calibrated using a standard fused silica specimen. Load control method was used with a maximum loading of 200 nN. The low peak loading was based on the consideration that the

maximum displacement during indentation should be no more than 10% of the coating thickness, and that high loading may result in micro-cracks in the coating, which is thought to be relatively brittle compared with metal coatings. To obtain good resolution, 15 measuring points were used during loading and 20 during unloading.

3. Results and discussions

The structural and morphological properties of the synthesized and annealed Ti-doped ITO thin film coatings were characterized *via* x-ray diffraction (XRD) and field emission scanning electron microscopy (FESEM) techniques and were discussed in our previous work [27]. The XRD results confirm the formation of body centred cubic bixbiyte structure with space group of *Ia3*/cubic similar to In_2O_3 (JCPDS card 06-0416). The ionic radiuses of tin (Sn^{4+}), Titanium (Ti^{4+}) and indium (In^{3+}) are 0.07, 0.06 and 0.09 nm, respectively. The small ionic radii of Sn^{4+} and Ti^{4+} imply that the crystalline features of In_2O_3 and/or ITO frameworks should not change if these elements are used as dopants. Grain sizes increase with the introduction of Ti dopants along with increasing annealing temperature, reaching the maximum value of 80 nm for the film prepared with 4 at% Ti concentration and post-annealed at 500°C. Therefore, we propose that enhancing the crystal growth and the preferred orientation of the 3-d metal doped ITO thin films could be attributed to introduction of Ti as a dopant for these thin films.

The FESEM images of the synthesized ITO and Ti-doped ITO films as deposited (150 °C) and after being annealed at 400, 500 and 600 °C show that the surfaces of all the thin films are smooth, homogeneous, and composed of uniform coalesced clusters, and show a grain structure demonstrating nanocrystalline features. However, the as deposited thin film of 4 at% Ti shows a smoother surface and possesses larger grains compared to those of pure ITO and 2 at% Ti-doped ITO, which may be attributed to the enhancement of crystallinity with Ti ratio.

3.1. Raman analysis

Raman spectroscopy was used to study the effect of Ti contents and annealing temperature on the electronic and mechanical properties of Ti doped ITO thin films. It is well known that ITO based materials have a body centred cubic structure that belongs to *Ia*3 space

group, similar to that of In_2O_3. Two types of cation are present in the ITO based structure: (1) 8 In^{3+} with 3 sides symmetry at b-sites and (2) 24 In^{3+} with 2-fold point symmetry at d-sites. Moreover, the 48 oxygen atoms in this structure occupy general e-sites with no symmetry. Thus, six possible vibration modes may be identified [28]:

$$4A_g + 4E_g + 14T_g + 5A_u + 5E_u + 16T_u$$

The A_g, E_g and T_g symmetry vibrations are Raman active and infrared (IR) inactive modes; whereas, T_u vibration modes are Raman inactive and IR active. The A_u and E_u vibration modes are inactive for both Raman and IR measurements. Figure 2 presents the results of Raman active modes for the Ti doped ITO thin films at 2% and 4% Ti concentrations after being annealed at the temperatures of 400, 500 and 600 °C. The observed vibrational modes correspond to 106, 135, 176, 275, 367, 432, 584, 633 and 704 cm^{-1} which represent an unequivocal finger print for In_2O_3 and/or ITO cubic structure These results are in good agreement with Raman active modes observed from In_2O_3 and ITO based materials, refer to [29, 30]. The peaks recorded at a wavenumber below 500 cm^{-1} are attributed by In-O stretching vibrational modes in ITO matrix. However, the line at 633 cm^{-1} are due to the overlapping of the contributions from In-O, Sn-O and O-Ti-O vibrational modes with frequencies of 630, 633 and 636 cm^{-1} respectively. Indeed, these observed vibrational modes in Ti doped ITO structure may be ascribed to a good incorporation of Ti and Sn dopants into the In_2O_3 lattice. It is also noticed that, along with the increase in annealing temperature from 400 to 500 °C, the intensity of the high frequency peaks at 633 and 704 cm^{-1} was gradually enhanced. However, the intensity of the low frequency peak at 175 cm^{-1} decreased. For the sample annealed at 600 °C, the intensity of the high frequency peaks decreased and the low frequency peak at 135 cm^{-1} disappeared. Increasing the annealing temperature up to 600 °C also led to the disappearance of the peaks at 367 and 432 cm^{-1}.

3.2. Atomic compositions and surface chemical bonding states

The elemental compositions of Ti doped ITO thin films were obtained *via* XPS survey scans. Figure 3 (a, b) shows the survey scan results for the synthesized Ti doped ITO thin films for both Ti contents. The photoelectron peaks for In3d, Sn3d, Ti2p, O1s, Cl2p and C1s in the

binding energy range of 0 - 1200 eV were observed. The XPS survey spectra confirm the existence of the principal elements (In, Sn, Ti, Cl and O), as well as carbon, in the related sample coatings. Table 1 lists the atomic compositions of the Ti doped ITO thin films at 2% and 4% Ti concentrations after being annealed at 400, 500 and 600 °C. The results imply that the surface elemental composition of the film materials was significantly affected by annealing temperature. As the annealing temperature increased, the ratio of atomic percentages of the principal elements (In, Sn and Ti) to oxygen on the surface of the thin film coatings decreased for both levels of Ti doping. At 600 °C the Ti2p and Cl2p signals were completely absent for both 2 and 4 at % Ti concentrations, respectively, indicating that surface oxidation is taking place at high temperature. As the oxygen content becomes higher at high temperatures, the surface oxidation layer should become thicker. In order to compensate for any charge shifts, the XPS energy scale was calibrated by the C1s (C-H) line at 284.60 eV (bonding energy).

The XPS spectra for these elements are shown in Figures 4-8. The surface chemical bonding states of the annealed Ti doped ITO films were characterised by de-convoluting the high resolution In3d, Sn3d, Ti2p, Cl2p and O1s photoelectron lines using the Gaussian distribution, in order to appraise analysis the possible chemical bonding states of these atoms in the composites. The parameters, derived from the analysis of the XPS spectra, are listed in Table 2 and include: the photoelectron lines, bonding states and their corresponding binding energies, full width at half maximum (FWHM) values and atomic percentages of the elemental compositions present in the films after being annealed at 400, 500 and 600 °C as evaluated from XPS curve fittings.

The de-convoluted curves of the high resolution XPS spectra of $In3d_{5/2}$ photoelectron lines are shown in Figure 4 (a, b). It is clear that the de-convoluted $In3d_{5/2}$ spectrum is assigned to three different bonding states in the range of 443.6 - 445.4eV. The lower energy peaks placed within the range 443.6 – 443.8 eV (labelled i) is linked to In° bonding state, precisely In-In bonds, while the mid energy peaks located in the range 444.1 – 444.6 eV (labelled ii) corresponds to In^{3+} bonding state from In_2O_3 [31, 32]. The higher energy peaks in the range 444.7 – 445.4 eV (labelled iii) could be attributed to the In-Cl bonds from InCl.

Figure 5 (a, b) displays the de-convoluted curves of high resolution XPS spectra for $Sn3d_{5/2}$ photoelectron lines. Three bonding states in the range of 485.6 - 487.2 eV have been allocated. The first components are obtained within the range 485.6 - 485.8 eV (labelled ‘i’)

correspond to Sn^{4+} in SnO_2, whereas the second features (labelled 'ii') observed in the range 486.0 - 486.5 eV are related to Sn^{2+} from SnO. It has been reported by Fan and Goodenough that the Sn3d peak for Sn^{2+} in SnO was seen at a binding energy around 0.5eV higher than that for Sn^{4+} in SnO_2 [33, 34]. The SnO phase is thermodynamically less stable than the SnO_2 phase; therefore, the Sn^{4+} is thought to be the predominant state in the ITO based materials. The last components (labelled 'iii') seen in the range 486.6 - 487.2 eV may be attributed to the $SnCl_2$ bonding state.

The Ti2p photoelectron lines of Ti doped ITO films are presented in Figure 6 (a, b). The curve fitting of Ti2p core level XPS spectra assigned three components within the energy range of 457.3-458.5 eV. The lower constituent in the energy range of 457.3 - 457.5 eV (labelled 'i') corresponds to Ti^{3+} in Ti_2O_3 bonding state [35]. The second component within the energy range 457.9 - 458.0 eV could be attributed to $TiCl_3$; while the higher energy components in the range 458.4 - 458.5 eV correspond to Ti^{4+} from TiO_2 [36].

The de-convolution of O1s spectra exhibits three sub-peaks within the energy range of 529.3 -531.8 eV as shown in Figure 7 (a, b). The first components in the range of 529.3 - 529.6 eV correspond to O-In bonds and O-Ti bonds, in In_2O_3 and Ti_2O_3. The second components within the range 530.3 - 530.8 eV are attributed to TiO_2 and SnO_2 bonding states. Finally, the other components in the range of 531.4 - 531.8 eV could be due to the existence of O-Sn bonds [31, 32, 36]. For In_2O_3-based oxide semiconductors, the role of oxygen vacancies (Vo) on the electrical properties has inspired significant debate. Using first principle calculations and density function theory, Agoston *et.al* reported that the oxygen vacancies exist in indium oxide lattice are shallow, suitable for generating free electrons in the conduction band. Existence of oxygen vacancies in indium oxide system and its derivative materials indicate experimentally that these defects are the major source of n-type conductivity [37].

Figure 8 (a, b) shows the results from curve fitting of high resolution XPS spectra for Cl 2p photon lines. Here also three components were obtained in the range of 197.6 – 199.9 eV. The first components are observed in the energy range of 197.6 - 198.0 eV (labelled 'i') related to InCl bonding state [38], the second components within 198.5 - 198.7 eV (labelled 'ii') may be

attributed to $SnCl_2$ bonding states, while the last components in the range of 199.6 – 199.9 eV (labelled 'iii') corresponds to $TiCl_3$ bonding states [36]. Table 2 details the de-convoluting results of the XPS data of spin coated Ti doped ITO samples as a function of Ti concentrations and annealing temperature.

3.3. Mechanical properties (hardness, Young's modulus and wear resistance)

The thickness of the TCO films prepared for this study is within the range of 300-400 nanometres. It has previously been reported that the indentation depth should be less than 10% of the film thickness to avoid substrate effects. Therefore, in order to determine the hardness and elastic modulus values for our Ti doped ITO thin films, the measurements were taken at a maximum indenter depth of around 13 nm, which is less than one-tenth our samples thickness.

Figure 9 (a, b) shows the load-displacement curves determined from the nanoindentation measurements corresponding to the Ti doped ITO samples of both Ti contents and after being annealed. It was reported by Jian and co-worker that establishment of cracking in films underneath the nanoindentor resulted in a distinct discontinuity in the loading part of the loading displacement curve [39]. In this study, the experimental nanoindentation results presented in Figure 9 (a, b) confirmed that continuous loading curves were obtained for all the films, indicating that the phenomenon of cracking was absent in the Ti doped ITO films at different Ti contents and annealing temperatures. Figure 10 shows typical load-displacement curves of the nanoindentation measurements. Hardness and Elastic (Young's) modulus can be calculated directly from the measurements of indentation load and penetration depth for both loading and unloading process. From a typical load-penetration depth (*p*-*h*) curve, maximum load, maximum displacement and unloading stiffness (also called contact stiffness *S*) can be determined. The value of how resistant solid matter is to deformation under an applied force is known as the hardness which can be calculated from the following relation:

$$H = \frac{P_{max}}{A} \quad (1)$$

Where P_{max} is the maximum load and A is the area of the hardness impression

Young's modulus can also be calculated from the values of unloading stiffness and contact area by the following relation:

$$S = \beta \frac{2}{\sqrt{\pi}} E_{eff} \sqrt{A} \quad (2)$$

Where β is a dimensionless constant taken as unity and E_{eff} can be defined as

$$\frac{1}{E_{eff}} = \left(\frac{1-\sigma^2}{E} + \frac{1-\sigma_i^2}{E_i} \right) \quad (3)$$

where σ and σ_i are the Poisson's ratio of the indenter and the thin film coating respectively. E_{eff} and E_i are the Young's modulus of the indenter and the thin film coating, respectively.

The hardness (*H*) and elastic modulus (*E*) values of the Ti doped ITO films derived from nanoindentation experiments are shown in Figure 11 (a, b). A difference is observed between the trends in the hardness results of the two sets of samples. For the 2 at% samples, the hardness decreased with increasing annealing temperature, changing from 6.6 to 6.3 GPa when the annealing temperature increased from 400 to 600 °C. In contrast, for the 4 at% samples, the hardness seems to stabilise around 6.8 GPa after annealing at different temperatures, only showing a slight decrease after annealing at 500 °C. Overall, the results show that the ITO films with higher Ti concentrations have the highest average hardness. The hardness of the Ti-doped ITO thin films measured in the present study are generally consistent with those reported by Zeng et.al (6.5 ± 1.6 GPa) for 250 nm thick sputtered ITO thin films onto glass substrate using a Berkovich indenter with 6 mN load [40]. Similar trends were also observed by Yen *et.al* for ZnO thin films deposited by atomic layer deposition on Si substrates and then post annealed at different temperatures. They suggested that the decreasing hardness of the ZnO thin films with increasing annealing temperature can be related to the increment of the grain size with increasing temperature [41]. Also, the reduction in the hardness could be ascribed to the changes in elemental compositions resulting from the diffusion process in the coatings, softening of the substrate, stress relaxations and formation of new phases. As such, the decrease in the hardness of 2 at% Ti-doped ITO films with increasing annealing temperature could be attributed to a number of different mechanisms. In this work, the samples were annealed in atmospheric

environment, so it was expected that the composition of the surfaces would change due to oxidation. Therefore, it is reasonable to assume that the change in the hardness of Ti doped ITO samples is induced by the difference in the oxygen content on the surface of the film with increasing temperature, as proved in the XPS results (section 3.1). These results are in general agreement with those reported by Biswas and co-authors, which show that there is a relation between the hardness and the oxygen contents in the ITO film materials. They found that when the oxygen content increased from 6 to 10 wt% in the precursor solutions, the hardness of the corresponding ITO films decreased from 9.6 ± 0.9 GPa to 1.6 ± 0.1 GPa [42]. Barna *et.al* and Petrov *et.al* reported that, oxygen, impurities and other defects may lead to grain refinement and then change the morphology of the films [43, 44]. As a summary, a higher annealing temperature leads to larger grain size (as mentioned previously in Section 3.1), which, when combined with substitutions, interstitials, and/or the formation of oxygen vacancies and other point defects, may cause a hardness decrement, although this effect is not so significant in our 4 at% samples. In relation to the annealing temperature increment, the Young's modulus of Ti doped ITO films decreased for the films of 2 at% Ti, while it increased for the films of 4 at% as shown in Figure 11 (a and b). However, both thin films with 2 at% and 4 at% Ti contents present similar Young's modulus in the range of 137 - 143 GPa, which is comparable to the reported results given by Zeng *et.al* (120 - 160 GPa) [38] and Chen and Bull (141 GPa)[25, 40].

Elastic modulus along with hardness of material can influence wear behaviour. The wear of a material coupled with elastic limit define the ability of this material to deform under an applied stress and regain its initial state without being deformed permanently [45]. The ratio, *H*/*E*, which is obtained from nanoindentation measurements can be used to evaluate the wear resistance of the coating. The larger this ratio is the higher the wear resistance will be [46]. The Ti doped ITO thin films exhibited a decrease in *H/E* values which are correlated to the reduction of wear resistance through high annealing temperature, as shown in Table 3. It is clear from Table 3 that both the hardness and Young's modulus depends on the annealing temperature. As discussed previously, the prepared Ti doped ITO thin films were annealed in air atmosphere resulting in changes of the composition of the sample surface due to oxidation process. Thus, the decrease in the hardness of Ti doped ITO samples along with increasing annealing temperature could be attributed to increasing the oxygen contents at the surface of the film. A similar trend for Young's modulus was observed with increasing annealing temperature. Thus, it is possible to

surmise that the annealing temperature exerts a negative effect on the mechanical properties of the Ti doped ITO film coatings. The *H/E* values in this study are in the range of 4.5×10^{-2} – 4.6×10^{-2} and 4.8×10^{-2} - 5×10^{-2}, for the films of 2 at% and 4 at%, respectively. These values represent a reasonable level of wear resistance, which is even better than other metal oxide ceramics with *H/E* values of 3×10^{-2} - 4×10^{-2} [47, 48].

4. Conclusions

Ti-doped ITO thin films were fabricated on glass substrates using a low cost and efficient sol-gel spin coating method. The effects of Ti concentrations (*i.e.*, 2 at% and 4 at% Ti) and annealing temperature (ranging from 400 - 600 °C) on the phonon vibrational modes, surface chemical bonding states and mechanical properties of Ti doped ITO thin films were studied using Raman spectroscopy, XPS and nanoindentation techniques. Raman analysis revealed the existence of ITO and/or In_2O_3 vibrational modes. By increasing the annealing temperature some peaks were inversely altered. The XPS results show that the main component atomic percentages such as In, Sn and Ti decreased as the annealing temperature increased from 400 to 600 °C, while the O atomic percentages increased. Also, at 600 °C, the Ti2p and Cl2p signals were completely absent for 2 at % and 4 at % Ti concentration, respectively, indicating that surface oxidation takes place at high temperature.

The nanoindentation load-displacement curves confirmed that all the films exhibited continuous loading curves, indicating that the phenomenon of cracking was absent in the Ti doped ITO films at both Ti contents. Variations in the hardness (*H*) and the elastic modulus (*E*) were observed with different Ti at% and annealing temperature. The hardness is within the range of 6.3-6.6 GPa and 6.7-6.8 GPa for 2 at% and 4 at% Ti content samples, respectively. In most cases the hardness values are negatively affected with increasing annealing temperature, and the films with higher Ti concentration in the ITO films possess the highest average hardness. Synthesized Ti-doped ITO thin films at different Ti contents show the same Young's modulus values in the range of 137 - 143 GPa. A combination of the highest *H* and *E* were achieved in the sample of 4% Ti content annealed at 600 °C. All the Ti-doped ITO films appear to possess high wear resistance. Combining with optimised control over the doping and annealing processes, the

results from this work are expected to help facilitate the engineering design of customizable Ti-doped ITO thin films for various industrial applications.

Acknowledgments

Hatem Taha wishes to thank the Iraqi government represented by the Ministry of Higher Education and scientific Research / University of Baghdad/ College of Ibn-Alhaitham for pure science for providing PhD scholarship.

References

[1] M.J. Kim, T.G. Kim, Fabrication of Metal-Deposited Indium Tin Oxides: Its Applications to 385 nm Light-Emitting Diodes, ACS Appl. Mater. Interfaces, 8 (2016) 5453-5457.
[2] K.L. Chopra, S. Major, D.K. Pandya, Transparent conductors—A status review, Thin Solid Films, 102 (1983) 1-46.
[3] A. Subrahmanyam, A. Rajakumar, M. Rakibuddin, T.P. Ramesh, M.R. Kiran, D. Shankari, K. Chandrasekhar, Efficacy of titanium doped-indium tin oxide (Ti/TiO 2–ITO) films in rapid oxygen generation under photocatalysis and their suitability for bio-medical application, Physical Chemistry Chemical Physics, 16 (2014) 24790-24799.
[4] C. Lee, Y. Ko, Y. Kim, Device Performances of Organic Light-Emitting Diodes with Indium Tin Oxide, Gallium Zinc Oxide, and Indium Zinc Tin Oxide Anodes Deposited at Room Temperature, J. Nanosci. Nanotechnol., 13 (2013) 8011-8015.
[5] M. Girtan, G. Rusu, G. Rusu, S. Gurlui, Influence of oxidation conditions on the properties of indium oxide thin films, Applied surface science, 162 (2000) 492-498.
[6] H.R. Fallah, M. Ghasemi, A. Hassanzadeh, H. Steki, The effect of annealing on structural, electrical and optical properties of nanostructured ITO films prepared by e-beam evaporation, Materials Research Bulletin, 42 (2007) 487-496.
[7] L. Kőrösi, S. Papp, S. Beke, B. Pécz, R. Horváth, P. Petrik, E. Agócs, I. Dékány, Highly transparent ITO thin films on photosensitive glass: sol–gel synthesis, structure, morphology and optical properties, Applied Physics A, 107 (2012) 385-392.
[8] R. Latz, K. Michael, M. Scherer, High conducting large area indium tin oxide electrodes for displays prepared by dc magnetron sputtering, Japanese Journal of Applied Physics, 30 (1991) L149-L151.
[9] S.Y. Lien, A. Nautiyal, S.J. Lee, Optoelectronic Properties of Indium–Tin Oxide Films Deposited on Flexible and Transparent Poly (dimethylsiloxane) Substrate, Japanese Journal of Applied Physics, 52 (2013) 115801.

[10] S. Kuznetsova, L. Borilo, Obtaining sol-gel by means of indium oxide thin films with added tin on glass substrates, Glass and Ceramics, 70 (2014) 429-433.
[11] J. George, C. Menon, Electrical and optical properties of electron beam evaporated ITO thin films, Surface and Coatings Technology, 132 (2000) 45-48.
[12] T. Maruyama, K. Fukui, Indium-tin oxide thin films prepared by chemical vapor deposition, Journal of applied physics, 70 (1991) 3848-3851.
[13] H. Ohta, M. Orita, M. Hirano, H. Tanji, H. Kawazoe, H. Hosono, Highly electrically conductive indium–tin–oxide thin films epitaxially grown on yttria-stabilized zirconia (100) by pulsed-laser deposition, Appl Phys Lett, 76 (2000) 2740-2742.
[14] C. O'Dwyer, M. Szachowicz, G. Visimberga, V. Lavayen, S. Newcomb, C.S. Torres, Bottom-up growth of fully transparent contact layers of indium tin oxide nanowires for light-emitting devices, Nature nanotechnology, 4 (2009) 239-244.
[15] L. Kőrösi, S. Papp, I. Dékány, Preparation of transparent conductive indium tin oxide thin films from nanocrystalline indium tin hydroxide by dip-coating method, Thin Solid Films, 519 (2011) 3113-3118.
[16] M. Mirzaee, A. Dolati, Effects of tin valence on microstructure, optical, and electrical properties of ITO thin films prepared by sol–gel method, J Sol Gel Sci Technol, 75 (2015) 582-592.
[17] T.O.L. Sunde, E. Garskaite, B. Otter, H.E. Fossheim, R. Saeterli, R. Holmestad, M.-A. Einarsrud, T. Grande, Transparent and conducting ITO thin films by spin coating of an aqueous precursor solution, Journal of Materials Chemistry, 22 (2012) 15740-15749.
[18] A. Amri, Z.T. Jiang, N. Wyatt, C.Y. Yin, N. Mondinos, T. Pryor, M.M. Rahman, Optical properties and thermal durability of copper cobalt oxide thin film coatings with integrated silica antireflection layer, Ceramics International, 40 (2014) 16569-16575.
[19] H.J. Lee, J.H. Hwang, K.B. Choi, S.-G. Jung, K.N. Kim, Y.S. Shim, C.H. Park, Y.W. Park, B.-K. Ju, Effective indium-doped zinc oxide buffer layer on silver nanowires for electrically highly stable, flexible, transparent, and conductive composite electrodes, ACS applied materials & interfaces, 5 (2013) 10397-10403.
[20] D.S. Bhachu, D.O. Scanlon, G. Sankar, T.D. Veal, R.G. Egdell, G. Cibin, A.J. Dent, C.E. Knapp, C.J. Carmalt, I.P. Parkin, Origin of high mobility in molybdenum-doped indium oxide, Chem. Mater., 27 (2015) 2788-2796.
[21] Z. Chen, W. Li, R. Li, Y. Zhang, G. Xu, H. Cheng, Fabrication of highly transparent and conductive indium–tin oxide thin films with a high figure of merit via solution processing, Langmuir, 29 (2013) 13836-13842.
[22] S.H. Chuang, C.S. Tsung, C.H. Chen, S.L. Ou, R.H. Horng, C.Y. Lin, D.S. Wuu, Transparent conductive oxide films embedded with plasmonic nanostructure for light-emitting diode applications, ACS Appl. Mater. Interfaces, 7 (2015) 2546-2553.
[23] J.v. Deelen, H. Rendering, M. Theelen, Z. Vroon, P. Poodt, A. Hovestad, Highly improved transparent conductors by combination of TCOs and metallic grids, IEEE PVSC, (2010) 992-994.

[24] R. Martínez-Morillas, R. Ramírez, J. Sánchez-Marcos, E. Fonda, A. de Andrés, C. Prieto, Huge Photoresistance in Transparent and Conductive Indium Titanium Oxide Films Prepared by Electron Beam–Physical Vapor Deposition, ACS applied materials & interfaces, 6 (2014) 1781-1787.
[25] J. Chen, S.J. Bull, Assessment of the toughness of thin coatings using nanoindentation under displacement control, Thin Solid Films, 494 (2006) 1-7.
[26] W.C. Oliver, G.M. Pharr, Measurement of hardness and elastic modulus by instrumented indentation: Advances in understanding and refinements to methodology, J Mater Res, 19 (2004) 3-20.
[27] Hatem Taha, Z. T. Jiang, David J. Henry, Amun Amri, Chun-Yang Yin,, M.M. Rahman, Improving the optoelectronic properties of titanium doped indium tin.oxide thin films, Semiconductor Science and Technology, accepted for publication (May 2017, SST-103414.R1).
[28] J.R. Ferraro, Introductory raman spectroscopy, Academic press, 2003.
[29] O.M. Berengue, A.D. Rodrigues, C.J. Dalmaschio, A.J.C. Lanfredi, E.R. Leite, A.J. Chiquito, Structural characterization of indium oxide nanostructures: a Raman analysis, Journal of Physics D: Applied Physics, 43 (2010) 045401-045404.
[30] C.Y. Wang, Y. Dai, J. Pezoldt, B. Lu, T. Kups, V. Cimalla, O. Ambacher, Phase stabilization and phonon properties of single crystalline rhombohedral indium oxide, Crystal growth and Design, 8 (2008) 1257-1260.
[31] A. Nelson, H. Aharoni, X-ray photoelectron spectroscopy investigation of ion beam sputtered indium tin oxide films as a function of oxygen pressure during deposition, Journal of Vacuum Science & Technology A, 5 (1987) 231-233.
[32] W.F. Wu, B.S. Chiou, S.T. Hsieh, Effect of sputtering power on the structural and optical properties of RF magnetron sputtered ITO films, Semiconductor science and technology, 9 (1994) 1242-1249.
[33] J.C. Fan, J.B. Goodenough, X-ray photoemission spectroscopy studies of Sn-doped indium-oxide films, Journal of Applied Physics, 48 (1977) 3524-3531.
[34] W.F. Wu, B.S. Chiou, Effect of oxygen concentration in the sputtering ambient on the microstructure, electrical and optical properties of radio-frequency magnetron-sputtered indium tin oxide films, Semiconductor science and technology, 11 (1996) 196-202.
[35] F. Werfel, O. Brümmer, Corundum Structure Oxides Studied by XPS, Phys Scr, 28 (1983) 92-96.
[36] C. Sleigh, A.P. Pijpers, A. Jaspers, B. Coussens, R.J. Meier, On the determination of atomic charge via ESCA including application to organometallics, J Electron Spectrosc Relat Phenom, 77 (1996) 41-57.
[37] P. Ágoston, P. Erhart, A. Klein, K. Albe, Geometry, electronic structure and thermodynamic stability of intrinsic point defects in indium oxide, J Phys Condens Matter, 21 (2009) 455801-455811.

[38] B.H. Freeland, J.J. Habeeb, D.G. Tuck, Coordination compounds of indium. Part XXXIII. X-Ray photoelectron spectroscopy of neutral and anionic indium halide species, Canadian Journal of Chemistry, 55 (1977) 1527-1532.
[39] S.R. Jian, Y.H. Lee, Nanoindentation-induced interfacial fracture of ZnO thin films deposited on Si(1 1 1) substrates by atomic layer deposition, Journal of Alloys and Compounds, 587 (2014) 313-317.
[40] K. Zeng, F. Zhu, J. Hu, L. Shen, K. Zhang, H. Gong, Investigation of mechanical properties of transparent conducting oxide thin films, Thin Solid Films, 443 (2003) 60-65.
[41] C.Y. Yen, S.R. Jian, G.J. Chen, C.M. Lin, H.Y. Lee, W.C. Ke, Y.Y. Liao, P.F. Yang, C.T. Wang, Y.S. Lai, J.S.C. Jang, J.Y. Juang, Influence of annealing temperature on the structural, optical and mechanical properties of ALD-derived ZnO thin films, Applied Surface Science, 257 (2011) 7900-7905.
[42] N. Biswas, P. Ghosh, S. Sarkar, D. Moitra, P.K. Biswas, S. Jana, A.K. Mukhopadhyay, Nanomechanical properties of dip coated indium tin oxide films on glass, Thin Solid Films, 579 (2015) 21-29.
[43] A. Barna, P. Barna, G. Radnoczi, F. Reicha, L. Toth, Formation of aluminium thin films in the presence of oxygen and nickel, Physica status solidi (a), 55 (1979) 427-435.
[44] I. Petrov, P. Barna, L. Hultman, J. Greene, Microstructural evolution during film growth, Journal of Vacuum Science & Technology A, 21 (2003) S117-S128.
[45] M.M. Rahman, Z.T. Jiang, Z.f. Zhou, Z. Xie, C.Y. Yin, H. Kabir, M.M. Haque, A. Amri, N. Mondinos, M. Altarawneh, Effects of annealing temperatures on the morphological, mechanical, surface chemical bonding, and solar selectivity properties of sputtered TiAlSiN thin films, Journal of Alloys and Compounds, 671 (2016) 254-266.
[46] A. Leyland, A. Matthews, On the significance of the H/E ratio in wear control: A nanocomposite coating approach to optimised tribological behaviour, Wear, 246 (2000) 1-11.
[47] D. Kenfaui, G. Bonnefont, D. Chateigner, G. Fantozzi, M. Gomina, J.G. Noudem, Ca 3 Co 4 O 9 ceramics consolidated by SPS process: optimisation of mechanical and thermoelectric properties, Materials Research Bulletin, 45 (2010) 1240-1249.
[48] D. Kenfaui, D. Chateigner, M. Gomina, J.G. Noudem, Texture, mechanical and thermoelectric properties of Ca3Co4O9 ceramics, Journal of Alloys and Compounds, 490 (2010) 472-479.

Table.1. Elemental compositions of Ti doped ITO thin films at 2 at% and 4 at% Ti concentrations after being annealed at different temperatures

Ti Concentration	Annealing Temperature °C	Atomic percentage of the elements					
		In	Sn	Ti	O	Cl	C
2 at%	400	8.0	1.9	4.4	37.7	1.0	47.0
	500	7.7	2.8	2.9	39.6	1.8	45.2
	600	7.1	1.6	0.0	50.8	1.0	39.5
4 at%	400	9.2	3.2	7.4	35.9	1.2	43.1
	500	8.3	2.1	5.0	39.7	1.6	43.3
	600	6.6	1.9	4.0	52.0	0.0	35.5

Table.2. Fitting results of the XPS data of Ti doped ITO films for the core level binding energies

Ti concentration %	Annealing temperature °C	Photoelectrons lines	Bonding states	Binding energy (eV)	FWHM (eV)	Percentages of the components %
2%	400	In 3d5/2	In°(In-In bonds)	443.7	1.1	49.5
			In_2O_3	444.4	1.2	41.9
			$InCl/InO_x$	445.1	1.3	8.6
		Sn3d5/2	SnO_2	485.8	1.3	45.0
			$SnO/SnO_x/Sn$	486.3	1.2	41.6
			$SnCl_2$	486.9	1.3	13.4
		Ti 2p3/2	Ti_2O_3	457.4	0.5	28.8
			TiO_2	457.9	0.5	43.7
			$TiCl_3$	458.4	0.5	27.5
		O 1s	TiO_2/In_2O_3	529.4	1.2	52.6
			InO_x/SnO	530.4	2.2	31.1
			Ti_2O_3/SnO_2	531.5	1.8	16.3
		Cl 2p3/2	InCl	198.0	1.3	32.7
			$SnCl_2$	198.6	1.2	32.1
			$TiCl_3$	199.7	1.4	35.2
	500	In 3d5/2	In°(In-In bonds)	443.7	1.2	59.4
			In_2O_3	444.3	1.0	24.0
			$InCl/InO_x$	444.9	1.2	16.6
		Sn3d5/2	SnO_2	485.8	1.2	61.7
			$SnO/SnO_x/Sn$	486.5	1.0	30.7
			$SnCl_2$	487.2	1.0	7.6
		Ti 2p3/2	Ti_2O_3	457.4	0.5	31.9
			TiO_2	457.9	0.6	58.6
			$TiCl_3$	458.5	0.3	9.5
		O 1s	TiO_2/In_2O_3	529.5	1.4	66.1
			InO_x/SnO	530.8	1.6	20.3
			Ti_2O_3/SnO_2	531.8	1.7	13.6
		Cl 2p3/2	InCl	197.9	0.7	46.6
			$SnCl_2$	198.5	0.9	23.4

			$TiCl_3$	199.6	1.0	30.0
		In 3d5/2	In°(In-In bonds)	443.6	1.4	72.1
			In_2O_3	444.5	1.1	15.6
			$InCl/InO_x$	445.2	1.8	12.3
		Sn3d5/2	SnO_2	485.7	1.3	41.2
			$SnO/SnO_x/Sn$	486.3	1.5	55.4
	600		$SnCl_2$	487.0	1.3	3.4
		O 1s	TiO_2/In_2O_3	529.4	1.3	41.8
			InO_x/SnO	530.6	2.1	41.5
			Ti_2O_3/SnO_2	531.6	2.2	16.7
		Cl 2p3/2	InCl	197.7	1	39.5
			$SnCl_2$	198.5	0.9	30.1
			$TiCl_3$	199.8	0.9	30.4
		In 3d5/2	In°(In-In bonds)	443.7	1.3	64.4
			In_2O_3	444.5	1.1	23.1
			$InCl/InO_x$	445.3	1.5	12.5
		Sn3d5/2	SnO_2	485.7	0.9	30.3
			$SnO/SnO_x/Sn$	486.3	0.8	37.7
	400		$SnCl_2$	486.9	1.2	32.0
		Ti 2p3/2	Ti_2O_3	457.5	0.8	25.0
			TiO_2	458.0	0.7	33.8
			$TiCl_3$	458.5	0.9	41.2
		O 1s	TiO_2/In_2O_3	529.6	1.2	58.7
			InO_x/SnO	530.7	1.7	25.9
			In_2O_3	531.7	1.7	15.4
		Cl 2p3/2	InCl	197.9	0.9	30.7
			$SnCl_2$	198.7	1.2	39.4
			$TiCl_3$	199.9	1.2	29.9
		In 3d5/2	In°(In-In bonds)	443.6	1.2	53.5
			In_2O_3	444.1	1.0	33.8
			$InCl/InO_x$	444.7	1.1	12.7
		Sn3d5/2	SnO_2	485.6	1.2	35.3
			$SnO/SnO_x/Sn$	486.0	1.2	40.7
4%	500		$SnCl_2$	486.6	1.3	24.0
		Ti 2p3/2	Ti_2O_3	457.4	0.8	41.9
			TiO_2	457.9	0.6	39.7
			$TiCl_3$	458.5	0.5	18.4
		O 1s	TiO_2/In_2O_3	529.3	1.2	63.0
			InO_x/SnO	530.3	1.7	23.8
			TiO_2/In_2O_3	531.4	1.7	13.2
		Cl 2p3/2	InCl	197.6	1.2	42.6
			$SnCl_2$	198.6	1.3	37.1
			$TiCl_3$	199.7	1.2	20.3
		In 3d5/2	In°(In-In bonds)	443.8	1.3	75.7
			In_2O_3	444.6	1.1	19.5
			$InCl/InO_x$	445.4	1.0	4.8
		Sn3d5/2	SnO_2	485.7	1.1	31.8
			$SnO/SnO_x/Sn$	486.1	1.2	44.6
	600		$SnCl_2$	486.7	1.2	23.6
		Ti 2p3/2	Ti_2O_3	457.3	0.7	43.0
			TiO_2	457.9	0.5	40.4
			$TiCl_3$	458.4	0.5	16.6
		O 1s	TiO_2/In_2O_3	529.4	1.3	66.3
			InO_x/SnO	530.5	1.8	23.5
			TiO_2/In_2O_3	531.6	1.7	10.2

Table.3. Mechanical properties of Ti doped ITO films after being annealed at different temperatures

Ti concentration (at%)	Annealing temperature °C	Hardness (GPa)	Young's modulus (GPa)	Wear resistance ($H/E \times 10^{-2}$)
2	400	6.6	143	4.6
	500	6.4	141	4.5
	600	6.3	139	4.5
4	400	6.8	137	5.0
	500	6.7	141	4.8
	600	6.8	143	4.8

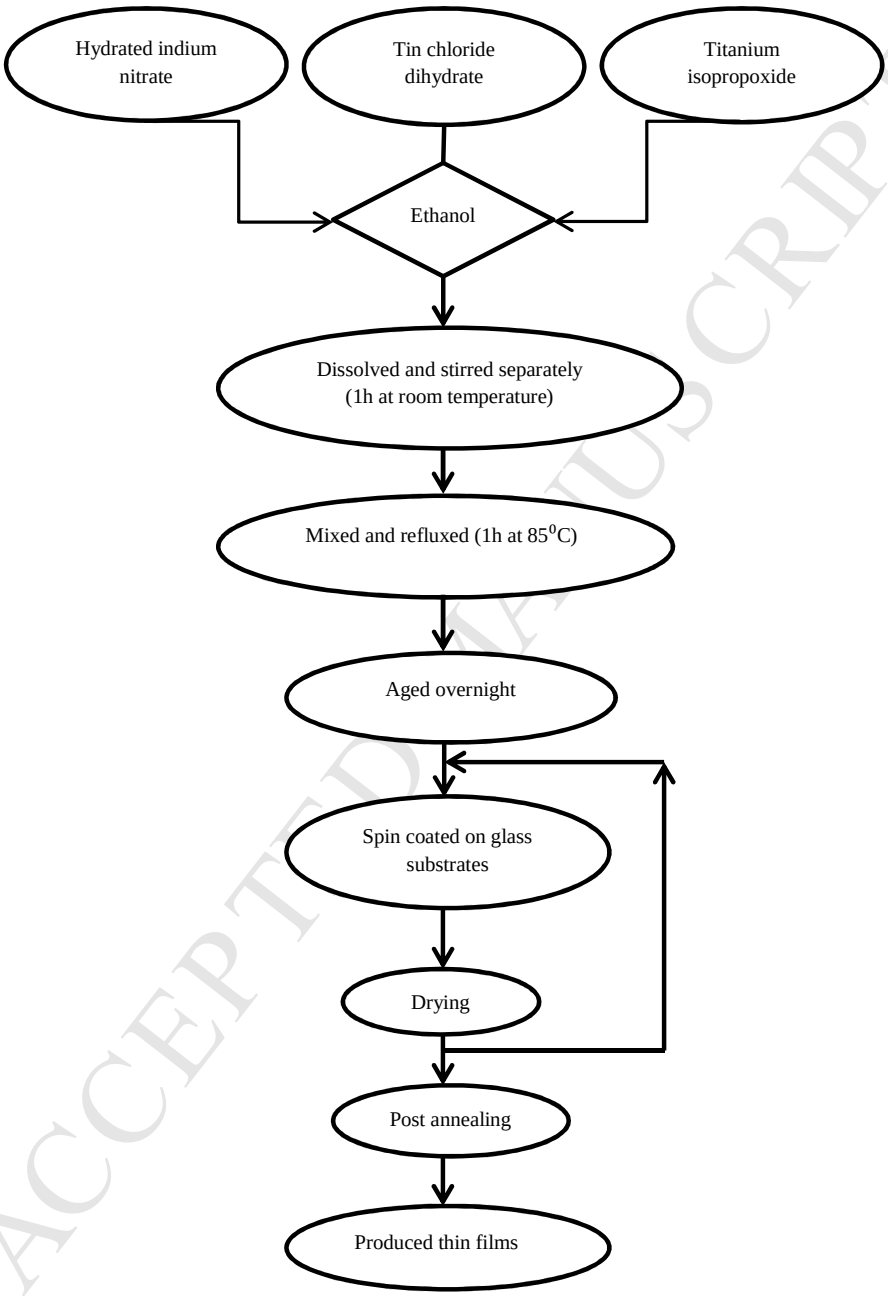

Fig.1. The flow chart for Ti doped ITO films preparation via sol-gel spin coating technique.

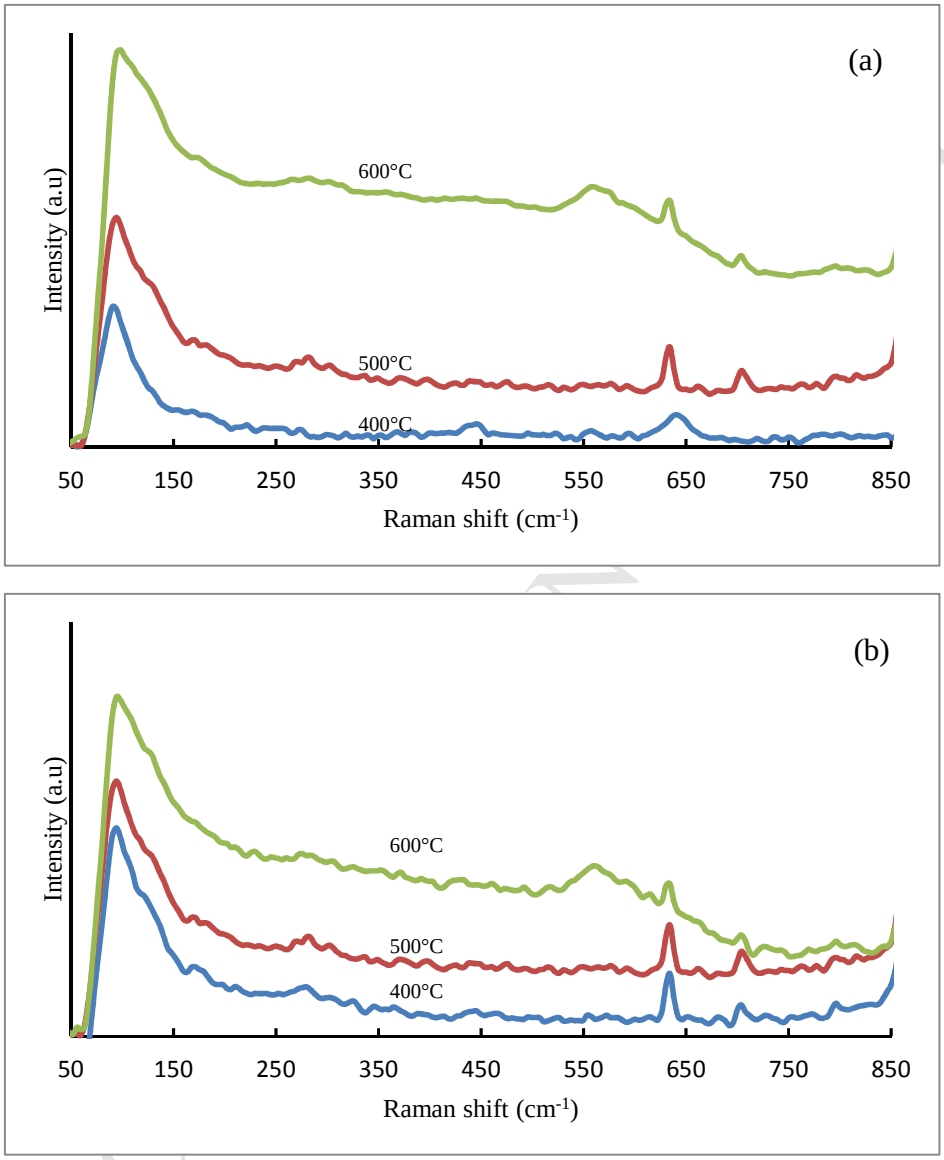

Fig.2. Raman shift of Ti doped ITO films (a): 2 at % and (b): 4 at % of Ti, annealed at different temperatures

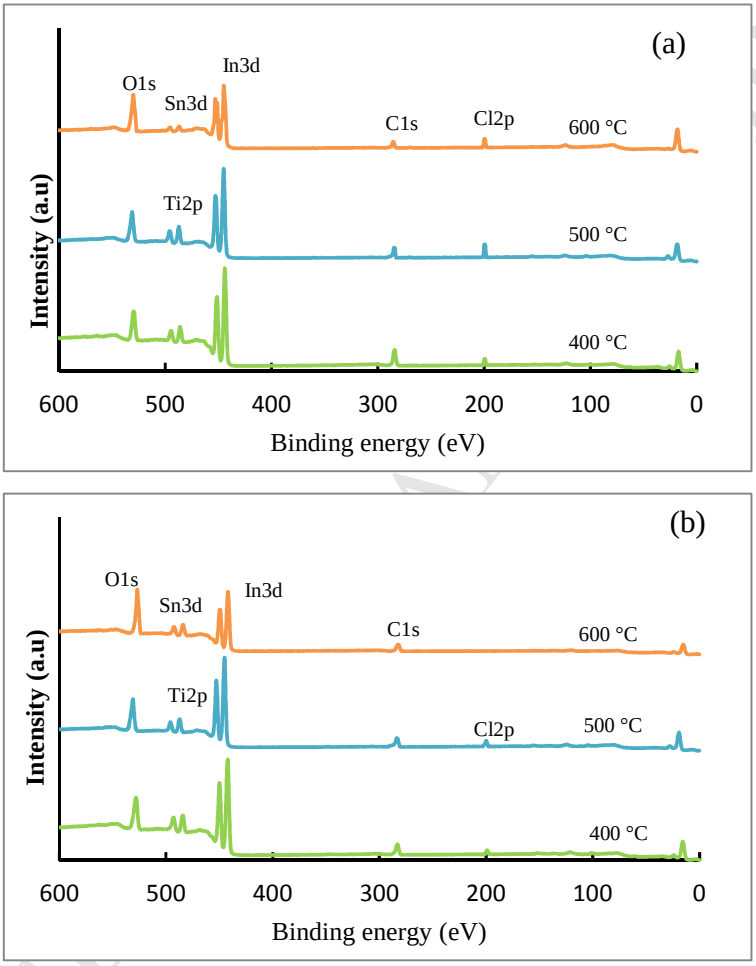

Fig.3. XPS survey scans of Ti doped ITO films (a): 2 at % and (b): 4 at % of Ti, annealed at different temperatures

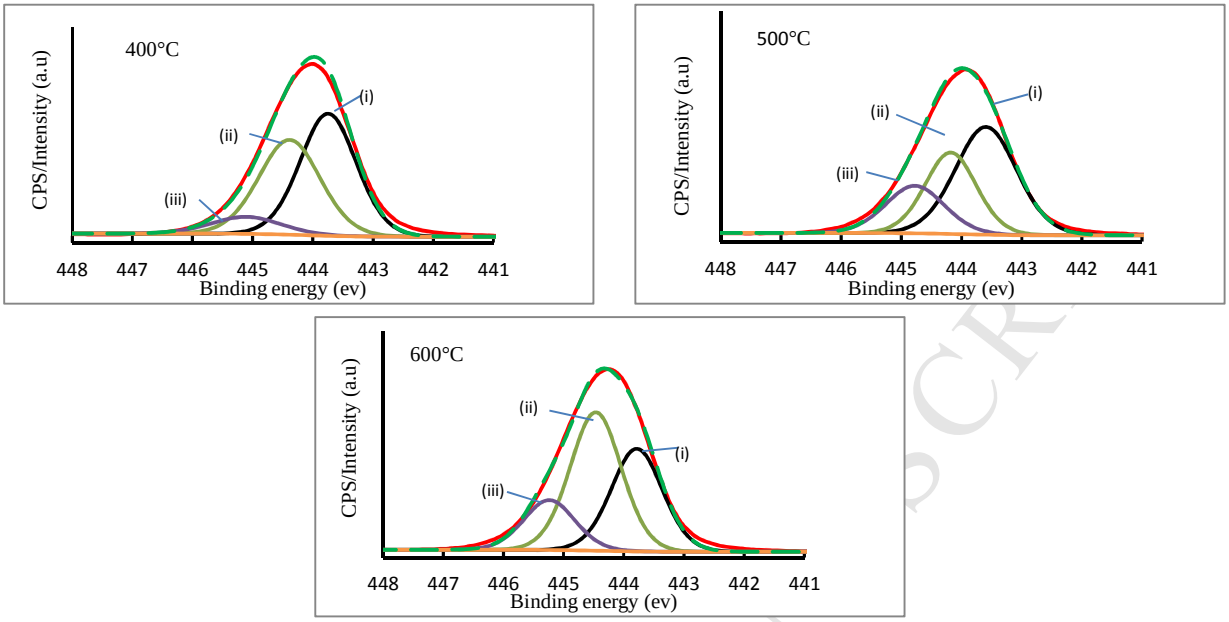

(a)

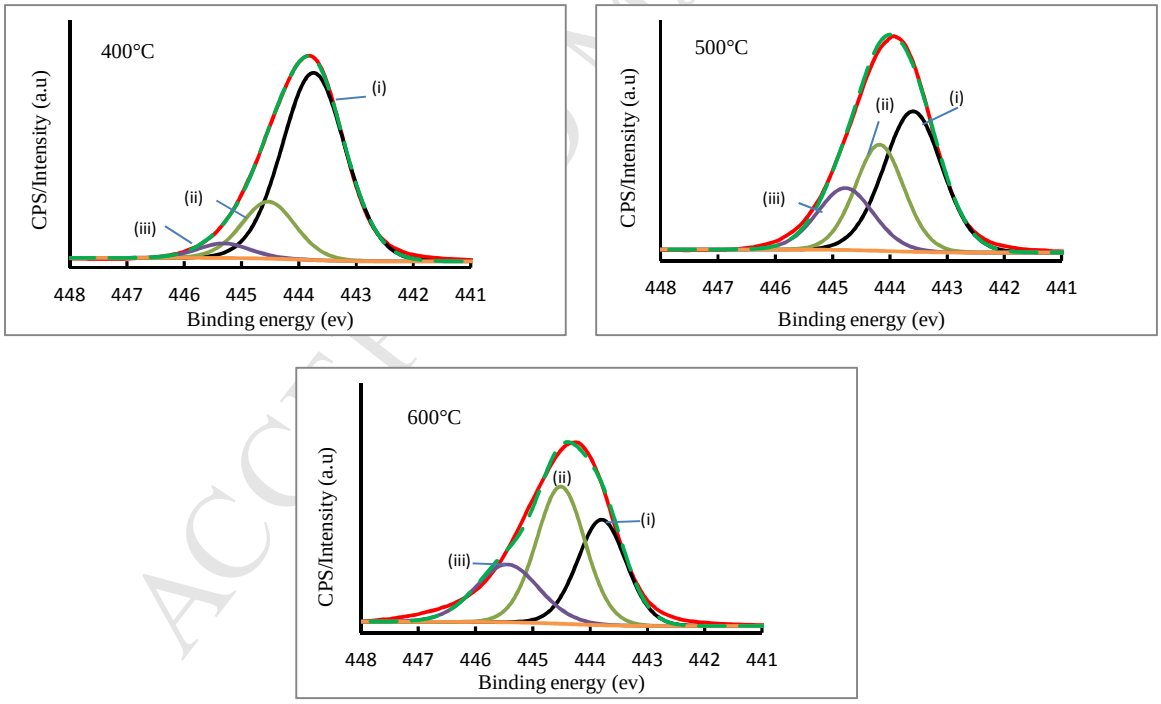

(b)

Fig.4. In3d XPS spectra of Ti doped ITO films (a): 2 at % and (b): 4 at % Ti, annealed at different temperatures

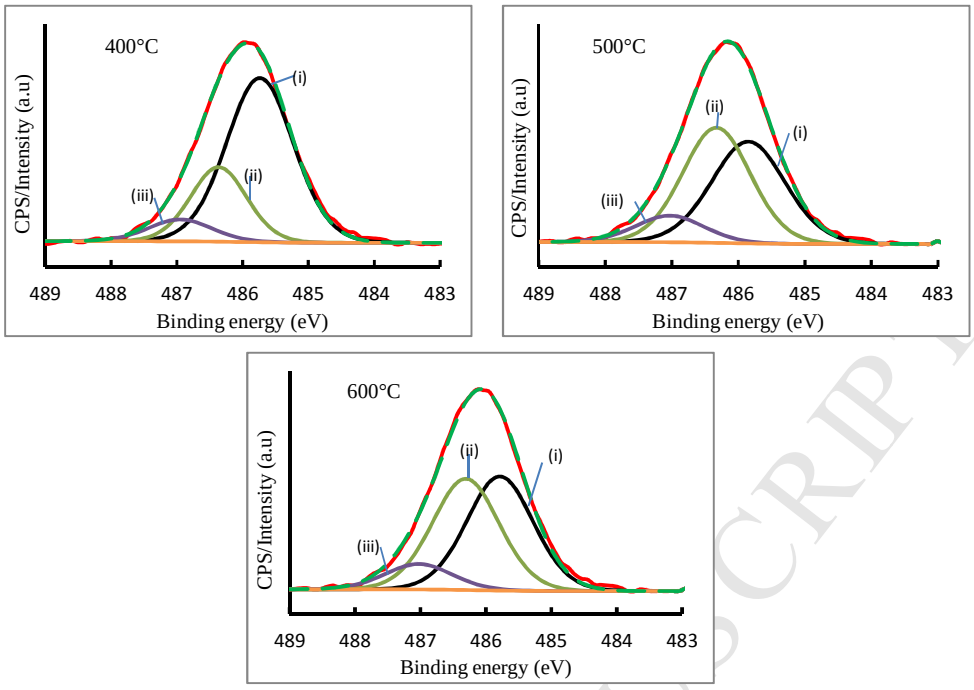

(a)

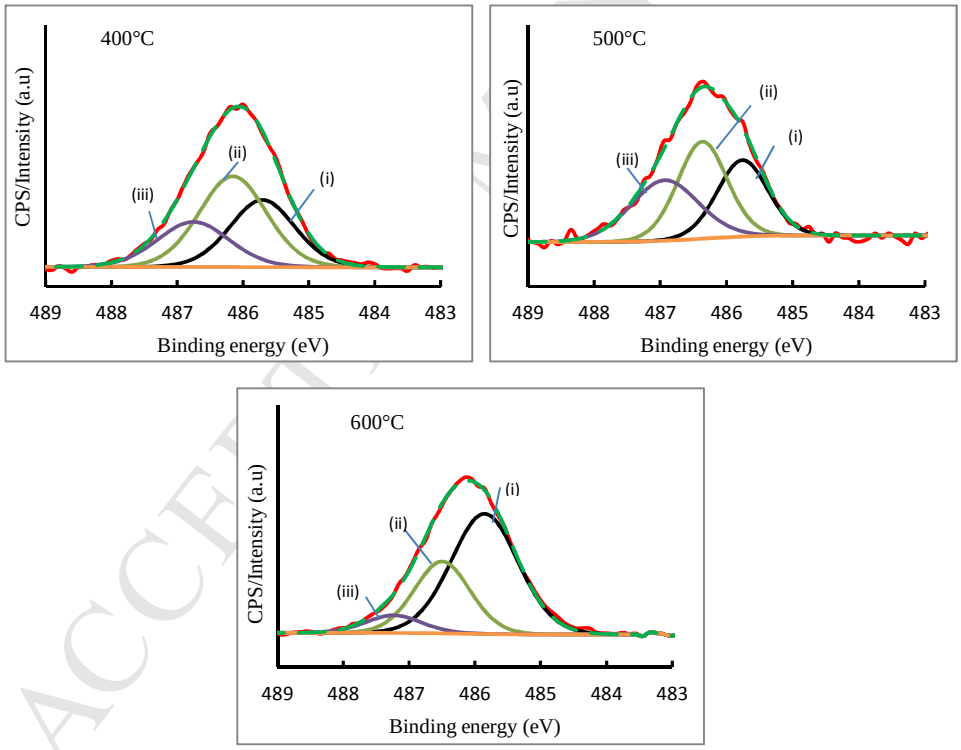

(b)

Fig.5. Sn3d XPS spectra of Ti doped ITO films (a): 2 at % and (b): 4 at % Ti, annealed at different temperatures

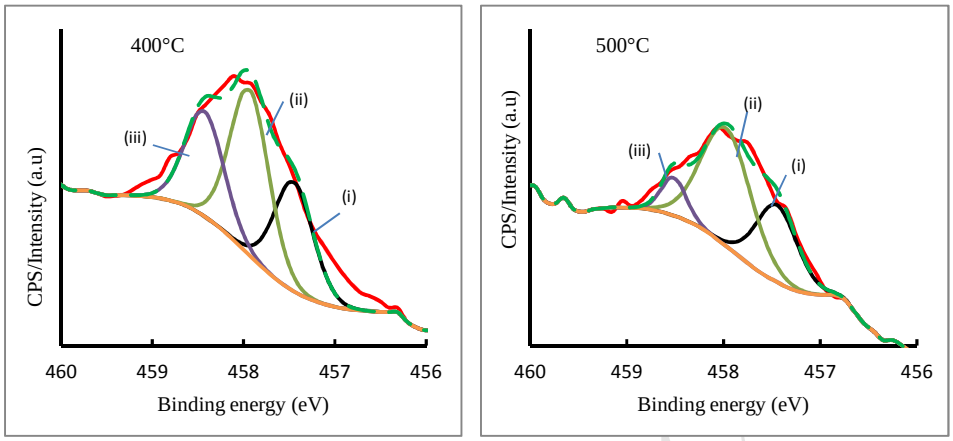

(a)

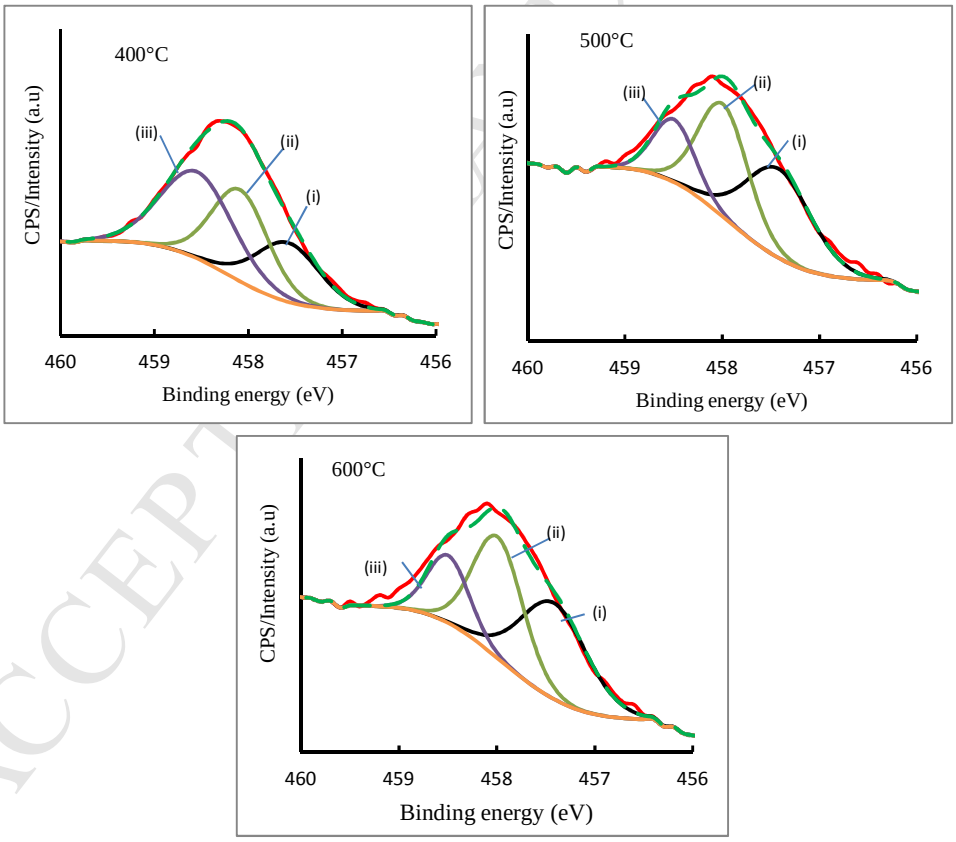

(b)

Fig.6. Ti2p XPS spectra of Ti doped ITO films (a): 2 at % and (b): 4 at % Ti, annealed at different temperatures

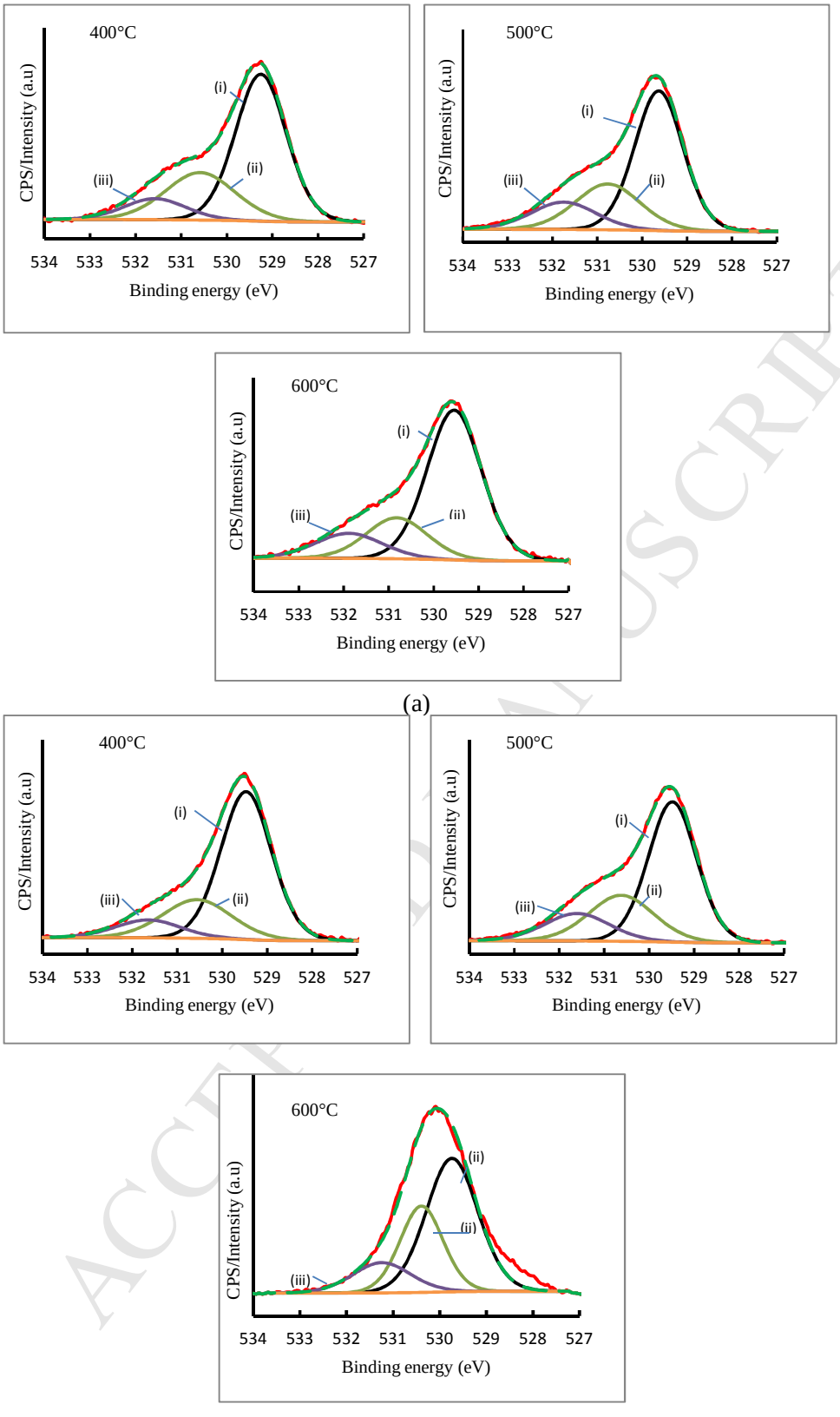

(a)

(b)

Fig.7. O1s XPS spectra of Ti doped ITO films (a): 2 at % and (b): 4 at % Ti, annealed at different temperatures

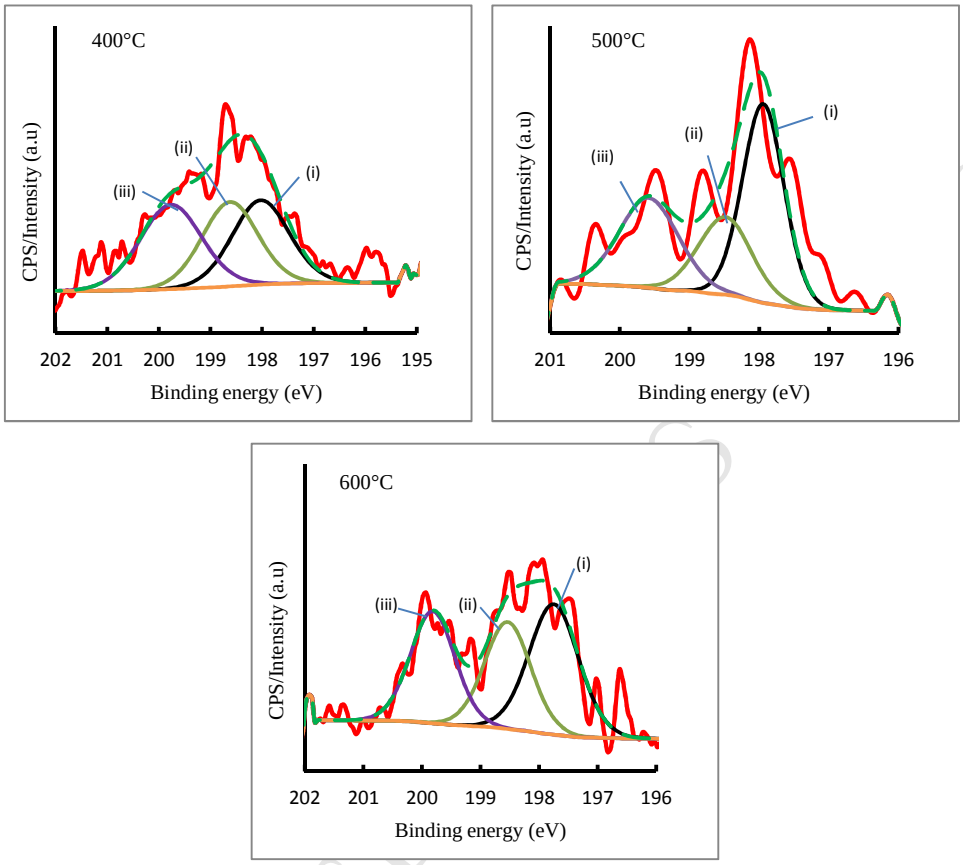

(a)

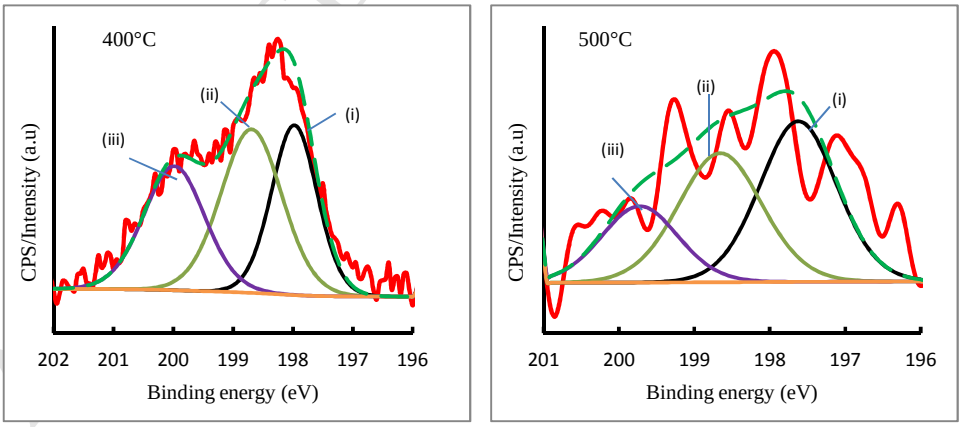

(b)

Fig.8. Cl2p XPS spectra of Ti doped ITO films (a): 2 at % and (b): 4 at % Ti, annealed at different temperatures

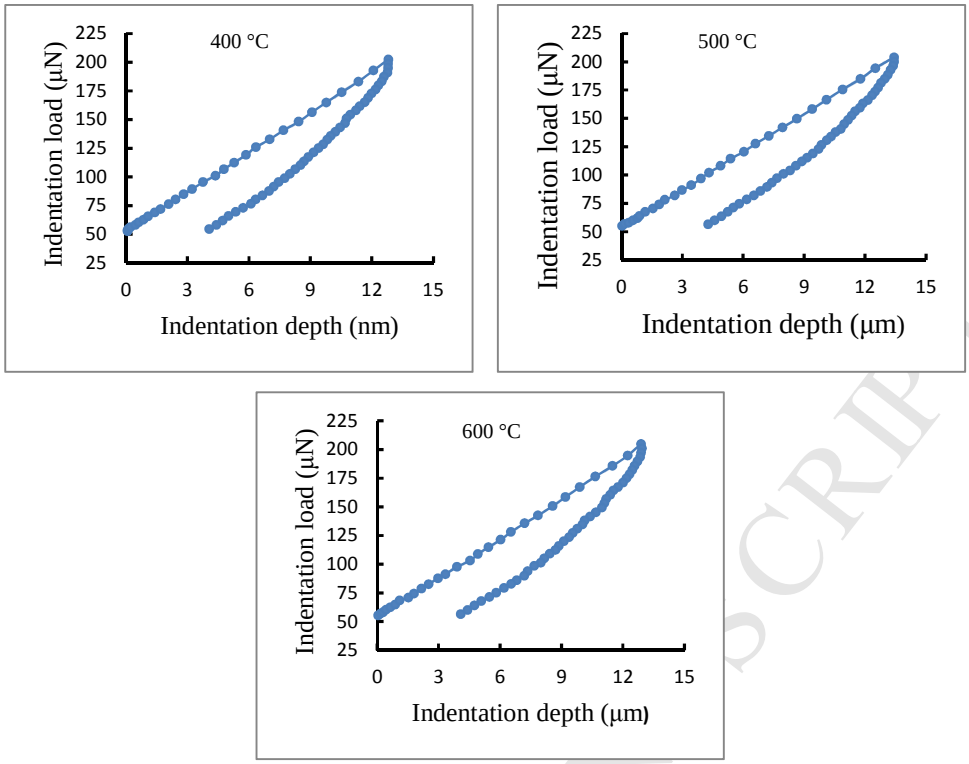

(a)

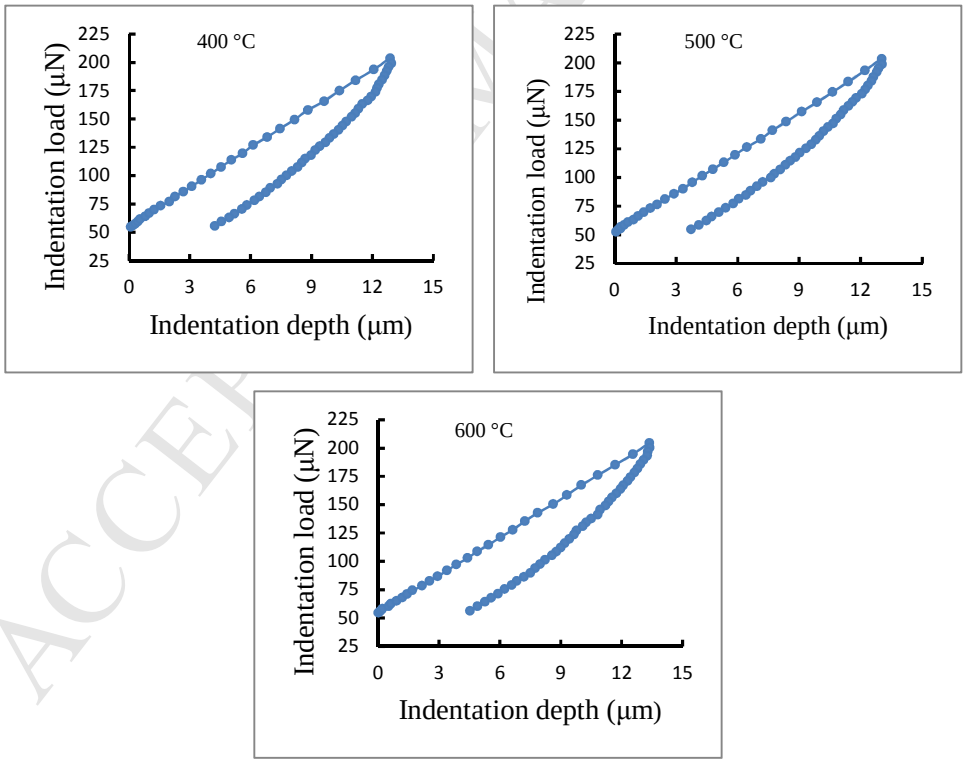

(b)

Fig.9. Load-displacement curves of Ti doped ITO films (a): 2 at % and (b): 4 at % Ti, annealed at different temperatures

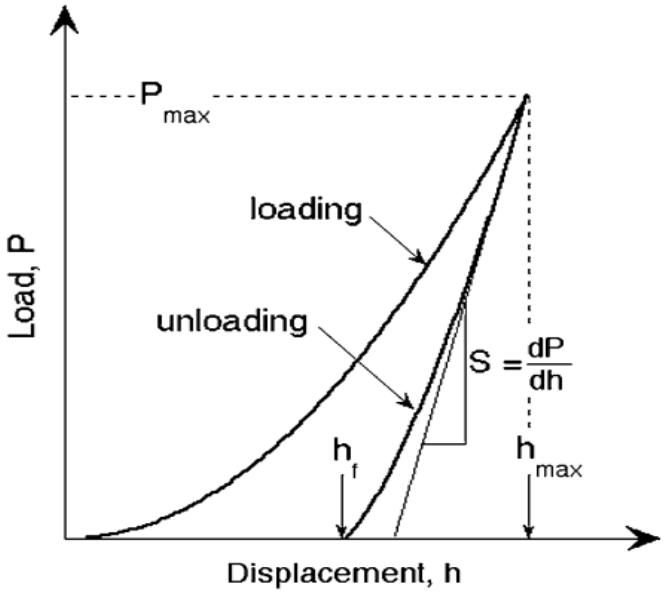

Fig.10. Typical loading and unloading curves of the nanoindentation measurements [26]

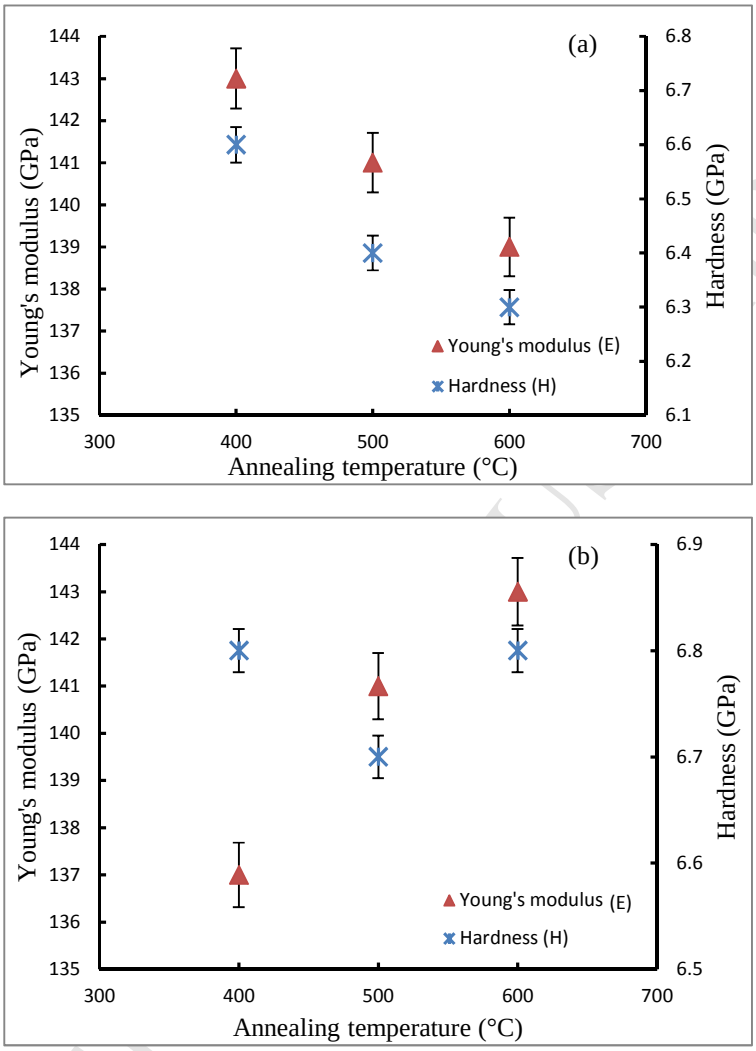

Fig.11. Hardness and Young's modulus of Ti doped ITO films (a): 2 at % and (b): 4 at % Ti, annealed at different temperatures

Highlights

- Ti-doped ITO thin films synthesized *via* spin coating technique
- Ti contents (2 and 4) at% and post annealing (400-600°) C were used.
- Surface chemical bonding states were determined *via* XPS.
- Hardness is in the range 6.3-6.8GPa.
- Young's Modulus is in the range 137-143GPa.